

Identification of Inhibitors against p90 Ribosomal S6 Kinase 2 (RSK2) through Structure-Based Virtual Screening with the Inhibitor-Constrained Refined Homology Model

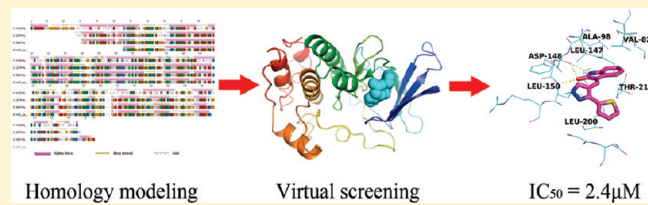
Shiliang Li,^{†,§} Yi Zhou,^{†,§} Weiqiang Lu,^{†,§} Ye Zhong,[†] Wenlong Song,[†] Kangdong Liu,[‡] Jin Huang,^{*,†} Zhenjiang Zhao,[†] Yufang Xu,[†] Xiaofeng Liu,^{*,†} and Honglin Li[†]

[†]State Key Laboratory of Bioreactor Engineering, Shanghai Key Laboratory of Chemical Biology, School of Pharmacy, East China University of Science and Technology, Shanghai 200237, China

[‡]The Basic Medical College, Zhengzhou University, Zhengzhou 450001, China

 Supporting Information

ABSTRACT: P90 ribosomal S6 kinase 2 (RSK2), which was shown to be overexpressed in human cancers, is a serine/threonine kinase and a potential target for cancer treatment. RSK2 comprises two terminal kinase domains (NTKD and CTKD) that can be inhibited by binding with different types of inhibitors at the ATP binding sites. In the absence of a crystal structure of RSK2, we constructed a model for the 3D structure of the RSK2 NTKD by homology modeling and stepwise constrained refinement with the reported inhibitors using a molecular docking method. Structure-based virtual screening was subsequently performed against a library containing commercially available compounds using the refined model. This resulted in the identification of seven novel RSK2 inhibitors with IC₅₀ values ranging from 2.4 to 14.45 μM.



INTRODUCTION

The p90 ribosomal S6 kinases (RSKs) are a family of serine/threonine protein kinases that are important downstream members of the Ras-mitogen activated protein kinase (MAPK) signaling pathway.¹ Four isoforms (RSK 1–4) have been identified in mammals, and RSK2 can specifically phosphorylate a variety of downstream proteins related to cell proliferation, growth, survival, and differentiation.² Furthermore, RSK2 is overexpressed in human breast, prostate, and lung cancer cells.³ Moreover, Coffin–Lowry syndrome (CLS), an X-linked semi-dominant syndrome characterized by severe psychomotoric retardation, facial and digital dysmorphisms, and progressive skeletal deformation in male patients, is associated with mutations in the RSK2 gene.^{4–7} Therefore, RSK2 is considered a promising target for treatment of cancer metastasis.⁸

RSK2 consists of two catalytically functional kinase domains connected by a linker of about 100 residues.⁹ The C-terminal kinase domain (CTKD) is reported to autophosphorylate Ser386 in the linker region and provides the binding site for the PDK1 kinase, which phosphorylates the N-terminal kinase domain (NTKD) of RSK2 at Ser227. This leads to subsequent activation of RSK2,¹⁰ which in turn phosphorylates various downstream substrates, such as cAMP-responsive element-binding 2 protein, histone H3, cell-cycle proteins Myt1 and Bub1, the tumor suppressor p53, nuclear factor of activated T cells (NF-AT), and other transcription factors.^{11–17} As an effector of the Ras-Erk pathway, RSK2 is necessary and sufficient to induce certain motile responses, and RSK2 inhibitors may play

a pivotal role in preventing cancer initiation and metastasis.¹⁸ However, crystal structures have not been determined for either the full-length human RSK2 or its NTKD,¹⁹ a fact that prompts various approaches for discovering novel and specific inhibitors of RSK2, especially through computational methods, such as structure-based virtual screening combined with homology modeling.²⁰ To date, a number of potent RSK2 inhibitors have been reported (as shown in Figure 1).²¹ Recently, dozens of novel RSK2 inhibitors were also discovered by our group using ligand-based virtual screening based on molecular similarity.⁸

To better understand the binding modes of the known RSK2 inhibitors and build a universal model at the atomic scale for RSK2 inhibitor discovery, we present here a homology model of RSK2 NTKD (residues 68–327), using the X-ray structures of mitogen- and stress-activated protein kinase (MSK1), RSK1 of *Homo sapiens*, and RSK2 NTKD of *Mus musculus* as the templates. Subsequently, to achieve the most reliable model that can be used to interpret the activity profiles of the available inhibitors, a stepwise constrained refinement procedure was performed by sequentially docking 9 known inhibitors into the ATP binding site of RSK2 NTKD with position-constrained energy optimization. Structure-based virtual screening was performed against the MayBridge chemical catalogue to verify the reliability of the final RSK2 model. As a result, out of 26

Received: June 1, 2011

Published: October 13, 2011

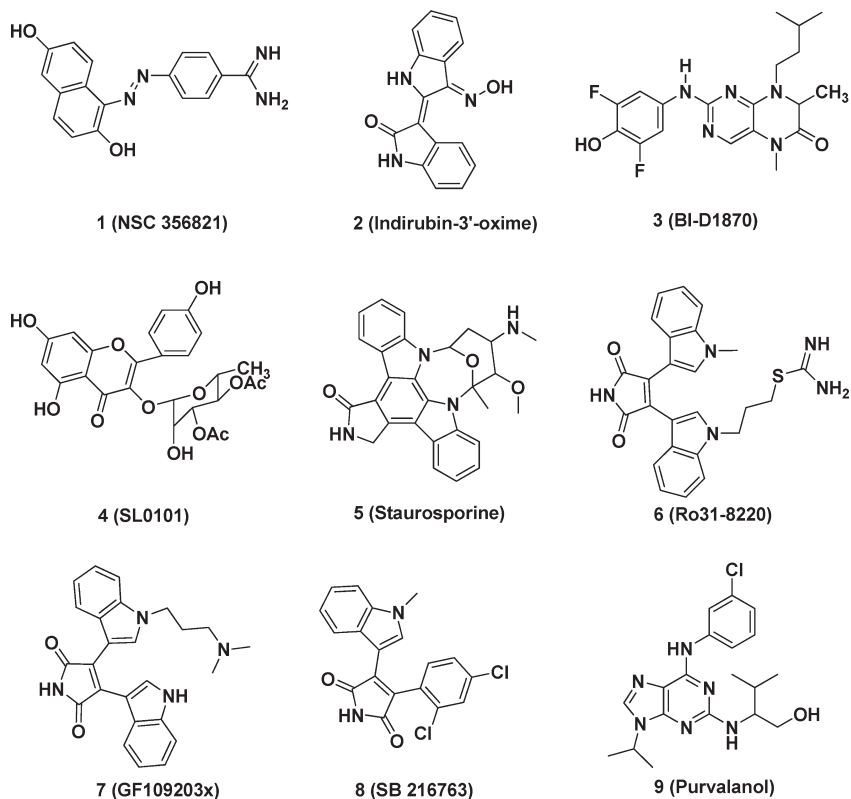


Figure 1. Chemical structures of the reported RSK2 NTKD inhibitors.

compounds tested, 7 novel RSK2 inhibitors were identified, and the most potent one showed an IC_{50} value of $2.4 \mu\text{M}$ against RSK2. These inhibitors might serve as new lead scaffolds for further development of tumor inhibitors through interrupting RSK2-mediated signaling pathways.

■ EXPERIMENTAL METHODS

Homology Modeling of RSK2 NTKD. The sequence of the human RSK2 NTKD (residues 68–327) was retrieved from the National Center for Biotechnology Institute (NCBI) with UniProtKB accession number P51812. The crystal structures of MSK1 and RSK1 of *Homo sapiens* (PDB IDs: 1VZO and 2Z7R) and RSK2 of *Mus musculus* (PDB ID: 3G51) were retrieved from the Protein Data Bank (PDB) and selected as the templates for homology modeling according to the results of BLAST search. Subsequently multiple sequence alignment (the overall sequence identities are over 55%) and RSK2 NTKD model construction were performed in Discovery Studio (DS) 2.1²² with default settings. The Ramachandran plot was prepared using Procheck,^{23–25} and a Profiles-3D test was conducted in DS 2.1 to evaluate the initial model.

Refinement of the Initial Model. To obtain a reliable model, structural refinement was performed with stepwise constrained optimization.²⁶ First, the initial model was optimized by energy minimization to correct disallowed torsion angles and to eliminate unfavorable atom–atom contacts using Prime²⁷ in Schrödinger 2009.²⁸ Then constrained optimization was carried out with the reported RSK2 inhibitors in the ATP-binding site. Using Glide,²⁹ five representative RSK2 inhibitors were sequentially docked into the ATP-binding site of the homology model according to their increasing molecule size

(as shown in Figure 1): 1 (NSC 356821), 2 (indirubin-3'-oxime), 3 (BI-D1870), 4 (SL0101), and 5 (staurosporine), which in turn is the parent compound for 6 (Ro31-8220), 7 (GF109203x), and 8 (SB 216763). At the end of each round of molecular docking, the residues around the binding site as well as the docked ligands were energetically minimized with position constraints to adjust the relative orientation and remove steric conflicts. During the refinement process, the pivotal hydrogen bonds formed between the ligands (groups labeled in Figure 1) and the hinge region (Asp148, Phe149, and Leu150) were also preserved. The docking refinement process was iterated with increasing molecule size until all the five ligands fit well into the refined ATP-binding site.

Virtual Screening. All molecular structures from the Maybridge Database³⁰ (~60 000 compounds) were prepared using LigPrep³¹ to add hydrogen atoms (protonation states corresponding to pH of 7.4), thereby generating stereoisomers and valid single 3D conformers. Hydrogen atoms and charges were added to the refined RSK2 NTKD structure in complex with staurosporine using the Protein Preparation Workflow in Maestro.²⁸ A grid-enclosing box was centered on the centroid of the ligand to enclose residues located within 14 Å of the ATP binding site, and a scaling factor of 1.0 was set to van der Waals (VDW) radii of those receptor atoms with a partial atomic charge of less than 0.25. The standard precision (SP) mode of Glide (with default parameters) was used to probe about 60 000 molecules for binding to the ATP-binding site. The top 1000 compounds were then redocked and scored with the Glide extra-precision (XP) method, which performs the conformational sampling more rigorously and uses a refined scoring function. The top 400 candidates (ranked by GlideScore) with the top 10 predicted binding poses preserved for each compound were retained for further analysis. To remove redundancies resulting

from similar structures, clustering techniques were employed using the Pipeline Pilot³² software to further reduce the size of the hit list. Finally, 300 molecules were reserved for further visual inspection. Several key binding interactions were additionally taken into consideration in the process of visual selection, including hydrogen-bonding interactions with Asp148 and Leu150 in the hinge region and hydrophobic interactions between the ligand and the hydrophobic region of the binding

site (comprising Leu74, Ala98, Phe149, Leu200, Phe79, Val82, Val131, Leu147, and Thr210). Meanwhile, structural diversity and VDW contacts were also factors contributing to this selecting procedure. In the end, 26 representative candidates were selected and purchased from the vendor for examination in a bioassay. The procedures of the structure-based virtual screening are shown in Figure 2.

Chemistry. All compounds were purchased from a commercial supplier (MayBridge) without further purification. HPLC analysis of the compounds assayed confirmed that the purity was ≥95%.

In-vitro Kinase Inhibition Assay. The ADP Quest assay (DiscoveRx) was performed in 96-well flat-bottom plates in 40 μL reaction volume according to the manufacturer's instructions. The kinase (20 ng, Millipore) in 30 μL of assay buffer (15 mM of HEPES, pH of 7.4, 20 mM of NaCl, 1 mM of EGTA, 0.02% of Tween 20, 10 mM of MgCl₂, and 0.1 mg/mL bovine γ-globulin) containing 25 μM of S6 peptide (AKRRRLSSLRA, Anaspec) was incubated for 20 min at room temperature with indicated concentrations of the compounds to be tested. Reactions were initiated by the addition of 10 μL of ATP to a final concentration of 10 μM and terminated after 60 min at room temperature by adding 20 μL of ADP reagent A and 40 μL of ADP reagent B. Ro31–8220 was used as a positive control. Compound solutions were prepared from DMSO stock and diluted with assay buffer for usage in the inhibition assay. The fluorescence signal detecting the amount of ADP produced, as a result of the enzyme's activity, was recorded using a Synergy 2 multimode microplate reader (BioTek) at an excitation wavelength of 530 nm and an emission wavelength of 590 nm at 30 min after the addition of ADP reagent B. The inhibition rate (%)

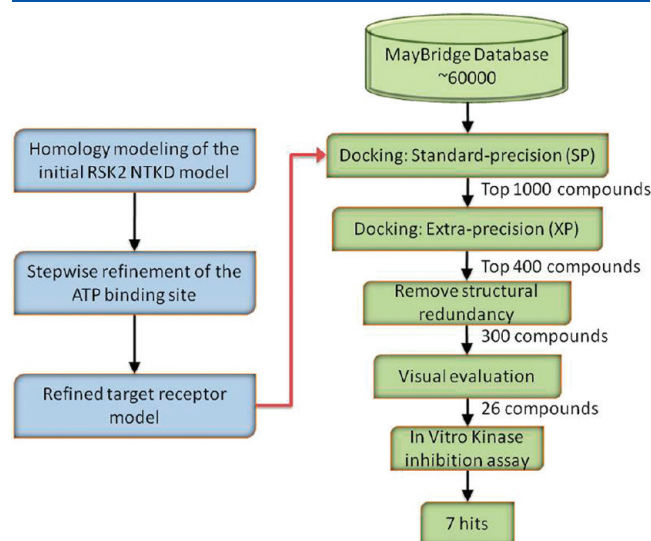


Figure 2. Procedures of the homology model building and structure-based virtual screening.

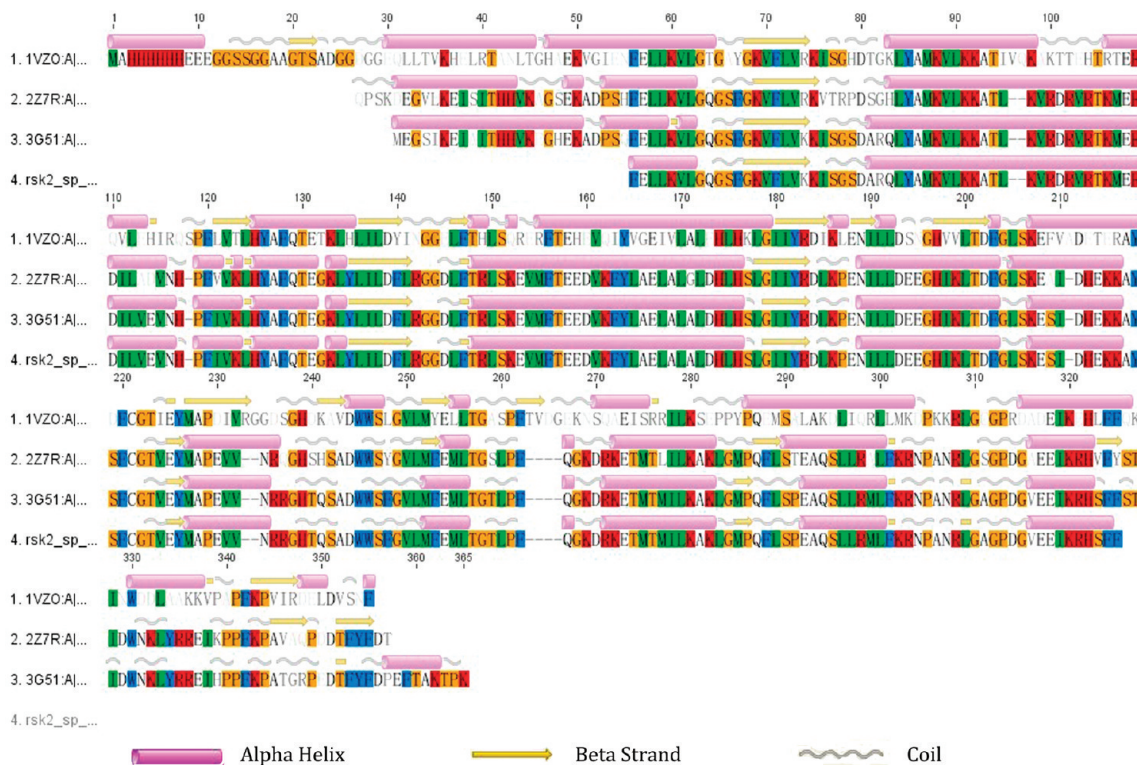


Figure 3. Multiple sequence-alignment results between the RSK2 NTKD and the template proteins. The amino acid residues of the templates and the target RSK2 NTKD sequences are colored by the Clustal method in Geneious.³⁴ The predicted α helix, β-strand, and coil regions are shown above the individual sequences of the alignment.

was calculated using the following equation:

$$\text{inhibition\%} = \left(1 - \frac{F_{590, \text{compd}}}{F_{590, \text{control}}} \right) \times 100\% \quad (1)$$

IC_{50} values were determined from the results of at least three independent tests and calculated from the inhibition curves. The accuracy of the in vitro assays was confirmed by the IC_{50} value of the control inhibitor Ro31–8220 at 10 nM, which was in agreement with the reported value.²¹

MTT Assays. The antiproliferation activity of RSK2 inhibitors discovered in this study was tested by the MTT assay as previously described with minor modification.³³ Human prostate carcinoma PC-3 cells (5×10^3) were seeded in 96-well plates with 200 μL of F-12K medium (Invitrogen) and incubated with compounds at the indicated concentration. Ro31–8220 served as a reference compound. After 48 h incubation, the cells were incubated with 10 μL of 5 mg/mL 3-[4,5-dimethylthiazol-2-yl]-2,5-diphenyl tetrazolium bromide (MTT) at 37 °C in a humidified incubator with 5% CO₂ for another 4 h. Then the formazan crystals were dissolved in 150 μL DMSO, and the absorbance was recorded at 570 nm by using a Synergy 2 multimode microplate reader (BioTek). The inhibition rate (%) was calculated as follows:

$$\text{inhibition\%} = \left(1 - \frac{F_{570, \text{compd}}}{F_{570, \text{control}}} \right) \times 100\% \quad (2)$$

IC_{50} values were determined from the results of at least three independent tests and calculated from the inhibition curves.

■ RESULTS AND DISCUSSION

Construction of the RSK2 NTKD Model. MSK1, RSK1 of *Homo sapiens* and RSK2 of *Mus musculus* were selected as the templates to construct the RSK2 NTKD model from 100 BLAST search hits according to their high sequence similarities (identities over 55%). The initial model for the RSK2 NTKD was constructed on the basis of multiple sequence-alignment analysis using DS 2.1 (Figure 3) by selecting the top-scored model out of five candidates. A Ramachandran plot (Figure 4) was generated to validate the model, indicating that more than 90% of the residues were located in the most favored $\varphi-\psi$ regions. A closer check of residues located in the nonfavorable regions revealed that they were far from the ATP-binding site, and there were no steric clashes between their side chains and the backbone. The results indicate that the model was comparatively reliable, this could also be confirmed by the result of Profiles-3D with the verification score (109.63) of the model being close to the expected highest score (118.175).

Stepwise Refinement of the Initial RSK2 NTKD Model. To get a more energetically reliable model compatible with each of the reported inhibitors, the initial model obtained by homology modeling was optimized by energy minimization using Prime to correct the disallowed torsion angles and eliminate unfavorable intramolecular contacts. Then the smallest inhibitor, NSC 356821, was manually docked into the ATP-binding site of the model using Glide with two mandatorily added pivotal hydrogen-bond constraints between the ligand and the hinge residues (Asp148 and Leu150). The most favorable binding mode was chosen for NSC 356821, and the residues within 8 Å around the compound in the binding site were chosen for energy

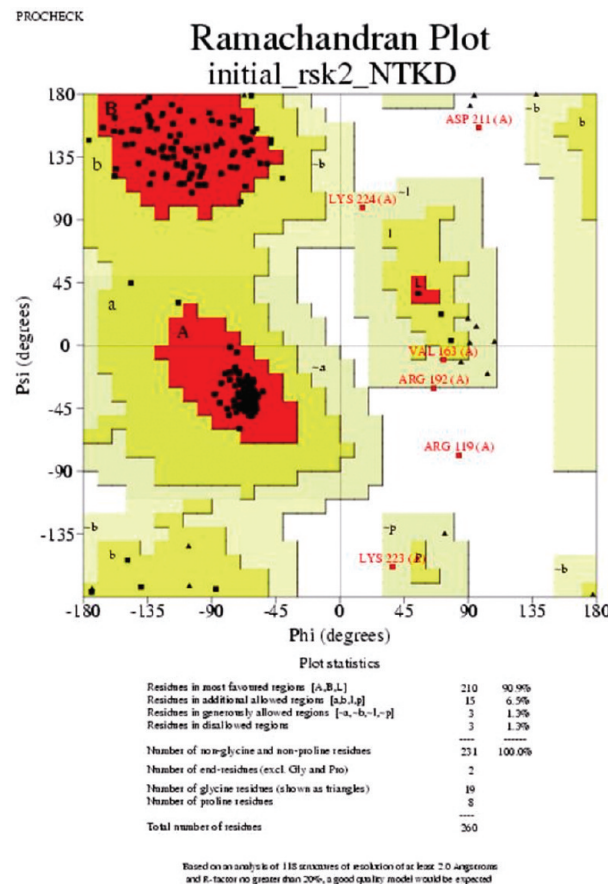


Figure 4. Ramachandran plot of the initial RSK2 NTKD model.

minimization in Prime. The hairclip-like glycine-rich flap (P-loop) and activation-loop regions were also refined in Prime using the loop refinement procedure with default parameters. The same procedures (molecular docking, energy minimization, and loop refinement) were iteratively applied with indirubin-3'-oxime, BI-D1870, SL0101, and staurosporine, according to increasing molecular size. In this way, it was ensured that the ATP-binding site of the final model was adjusted to accommodate these inhibitors with various molecular sizes.

The conformational changes of the ATP-binding site after each refinement iteration are shown in Figure 5. As seen in Figure 5A, the orientations of the binding site residues around NSC 356821 undergo obvious changes, especially in the case of Gln76, Phe79, Lys100, Phe149, Asp211, and Lys216, resulting in a more open ATP-binding pocket to accommodate larger inhibitors. For example, the active-site DFG (Asp-Phe-Gly) motif residue Asp211 as well as the residues around it integrally moves “backwards”, leading to a deeper ATP-binding pocket to facilitate inhibitor fitting to the cave.

Compared with the NSC 356821 model, the positional variations for the binding site residues are not obvious in the indirubin-3'-oxime refined model except for the P-loop located on the edge of the active pocket (as shown in Figure 5B). In the BI-D1870 model (Figure 5C), most of the orientations of the residues remain unchanged from the indirubin-3'-oxime model, with the exception of Lys72, Leu74, Lys100, and Phe149. The side chains of Leu74 and Phe149 undergo obvious orientation changes to form hydrophobic interactions with the

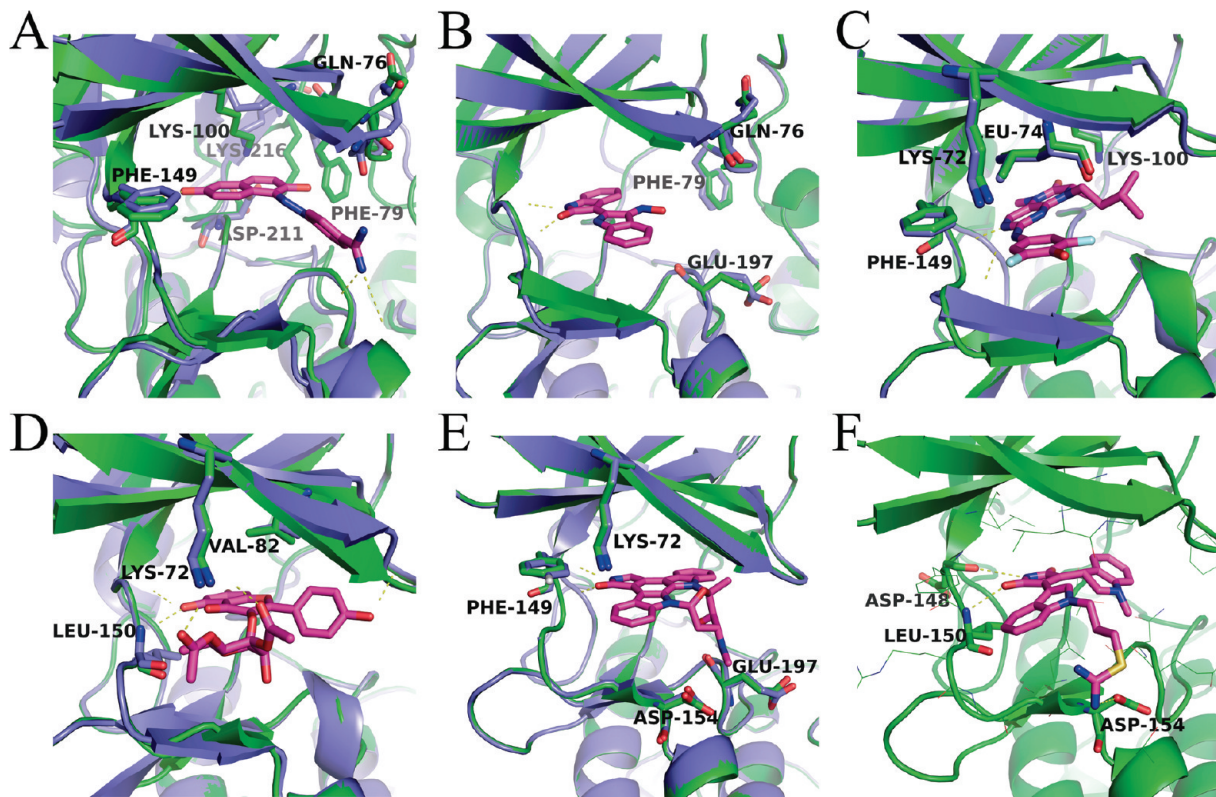


Figure 5. Detailed description of the subtle changes in the ATP binding site during the refinement process: (A) The initial RSK2 NTKD model (blue) is superimposed onto the NSC 356821 model (green); (B) The NSC 356821 model (blue) is superimposed onto the indirubin-3'-oxime model (green); (C) The indirubin-3'-oxime model (blue) is superimposed onto the BI-D1870 model (green); (D) The BI-D1870 model (blue) is superimposed onto the SL0101 model (green); (E) The SL0101 model (blue) is superimposed onto the staurosporine model (green); (F) The refined model in complex with RO31-8220. All the ligands are shown in stick mode and colored in purple. Important residues are shown as sticks in each model with the same color for corresponding models. Hydrogen atoms are not shown for clarity. Hydrogen bonds are shown as yellow dashed lines.

difluorobenzene group of BI-D1870. The orientations of Lys72 and Leu150 are also adjusted in the SL0101 model to form two hydrogen bonds with the acetyl groups in SL0101. Besides, the conformation of the P-loop in Figure 5B changes significantly after energy minimization. In Figure 5E, the residues within the ATP-binding site in the staurosporine model are repelled outward in order to accommodate this largest ligand.

During the position-constrained energy minimization, the ATP-binding site residues are subject to smaller or larger conformational changes. For example, the orientation of Phe79 is different in the NSC 356821 and the staurosporine models. To ensure that the nine reported inhibitors can fit well with the proposed model, all of them were docked into the final optimized structure and the receptor–ligand interaction were optimized simultaneously (interligand interactions were excluded) to make sure that the final model can accommodate all active inhibitors. At the same time, pivotal hydrogen bonds or salt-bridge interactions with key residues such as Asp148 and Leu150, which are located in the hinge region of the ATP-binding site and are proposed to be the two most important residues of the binding site, were forced to be preserved. As a verification test, Ro31-8220, which is also used as the positive control inhibitor in the subsequent bioassay test, was docked into the final model and exhibited a binding mode similar to that of staurosporine (Figure 5F).

Structural Analysis of the RSK2 NTKD Model. Overall Structure. The initial RSK2 NTKD model was aligned onto the

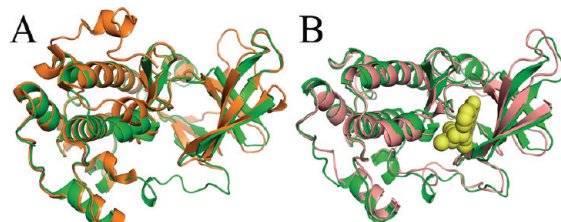


Figure 6. Structure of the RSK2 NTKD model. (A) The RSK2 NTKD initial model (green) is aligned to the template X-ray structure of RSK2 of *Mus musculus* (orange). (B) The RSK2 NTKD initial model (green) is aligned to the final RSK2 NTKD model (pink). The proteins are rendered in cartoon, and the staurosporine structure is shown as a yellow CPK model.

three templates (1VZO, 2Z7S, 3G51) used for homology modeling (Figure 6A), which—like all kinases—comprise two lobes and a cleft. The large lobe is composed of a three-stranded antiparallel β -sheet and a five-helix bundle, while the small lobe has a five-stranded antiparallel β -sheet. The cleft, which is located between the two lobes, is occupied by the ATP-binding site. The hinge region defines the interior of the ATP-binding site and links the two lobes. There are several obvious differences between the initial and the final refined models (Figure 6B). The P-loop went through a significant conformational change to accommodate larger inhibitors and facilitate the extra interactions.

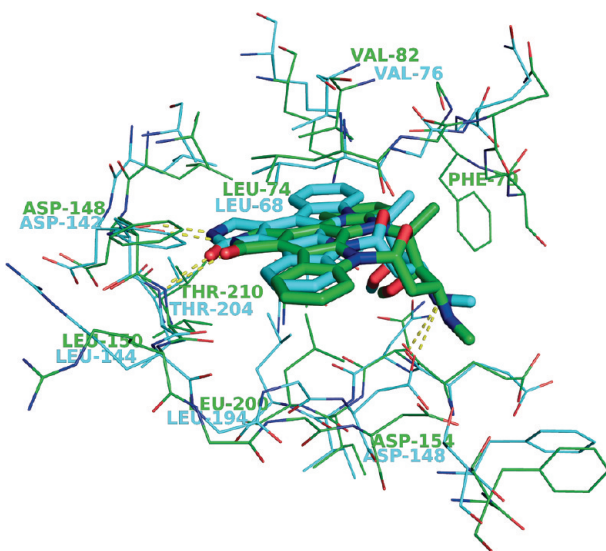


Figure 7. Comparison of the ATP-binding sites in the RSK2 NTKD model and the template RSK1 X-ray structure. Superimposition of the residues within 6 Å of the ligands of the RSK2 NTKD model (green carbon) and the template RSK1 X-ray structure (cyan carbon). Both of the two structures are drawn in lines with staurosporine rendered in stick mode. Oxygen atoms are colored red and nitrogen atoms blue. Hydrogen bonds are shown as yellow dashed lines.

Comparison of the ATP-binding Site of the Template and the RSK2 NTKD Model. Staurosporine has inhibitory activities against a wide range of protein kinases and is a potent but nonspecific RSK family inhibitor.²¹ We compared the binding modes of staurosporine between the RSK1 X-ray structure and the refined RSK2 NTKD model (Figure 7). Most of the residues, especially the conserved ones, within 6 Å of the ligand in the ATP-binding site, remain in similar orientations. Two hydrogen bonds form between staurosporine and the RSK2 NTKD model: the oxygen atom of the γ -butyrolactam moiety acts as hydrogen-bond acceptor for the Leu150 amide, while the nitrogen atom acts as hydrogen-bond donor for the main chain carbonyl oxygen on Asp148. Moreover, the secondary amine connected to the tetrahydropyran is protonated and forms a strong salt-bridge with the carboxylate group of Asp154. Favorable hydrophobic contacts, including interactions between the phenyl group of staurosporine and the side-chains of Leu200 and Leu74 as well as with Phe79, Thr210, and Val82, are also observed. Similar interactions can be observed in the X-ray structure of RSK1 in complex with staurosporine (Figure 7), indicating that the refined model of the RSK2 NTKD is comparatively reliable for interpreting the activity profiles of the known and novel RSK2 inhibitors in terms of binding poses.

Structure-Based Virtual Screening and Binding-Mode Analysis of Novel RSK2 Inhibitors. Out of the 26 candidates tested, 7 compounds were identified to exhibit moderate activities against RSK2, with IC₅₀ values ranging from 2.4 to 14.45 μ M (as shown in Table 1). With a success rate of 27% in our virtual screening approach, the results are encouraging. Furthermore, we tested the in vitro antiproliferative activities of the seven newly identified RSK2 inhibitors against PC-3 tumor cells. Four of the compounds demonstrated moderate antiproliferative activity (as shown in Table 1). To investigate the structural basis for the binding modes of these novel inhibitors in the RSK2 ATP-binding site, we scrutinized the binding poses by means of molecular

Table 1. Structures of the Seven Inhibitors, Their Inhibitory Activities against Rsk2 Kinase, and Their Antiproliferative Activities against PC-3 Tumor Cells

Compound.	Structure	IC ₅₀ (μ M) ^a (RSK2 kinase)	IC ₅₀ (μ M) ^b (PC-3)
10		2.4	11.42
11		3.89	39.42
12		5.01	15.15
13		7.76	91.78
14		9.33	ND
15		12.88	ND
16		14.45	ND
Ro31-8220		0.010	1.74

^aIf the inhibition rate at 10 μ M was larger than 30%, IC₅₀ values were determined from the results of at least three independent measurements of RSK2 kinase activity. ^bRelative inhibition rates of antiproliferative activity were determined by MTT assays. The final concentration of the compounds was 100 μ M. IC₅₀ values were determined from the results of at least three independent tests with the PC-3 cell line in antiproliferative assays. Attempts to determine IC₅₀ values were made if the inhibition rate at 100 μ M was larger than 40%. ND: not determined.

docking (Figure 8). Figure 8A shows the predicted binding pose of compound 10 in the ATP-binding site. The butyrolactam moiety of compound 10 forms hydrogen bonds with Asp148 and Leu150 of the hinge region, and the phenyl moiety fits well into the hydrophobic region comprising Val82, Ala98, Leu147, Leu200, and Thr210. Moreover, the thiophene moiety can also make numerous VDW contacts with residues Leu200 and Val82. By forming hydrogen bonds with the backbone oxygen atom of Asp148 and the backbone nitrogen atom of Leu150, compound 11 has the same binding mode as compound 10 and displays

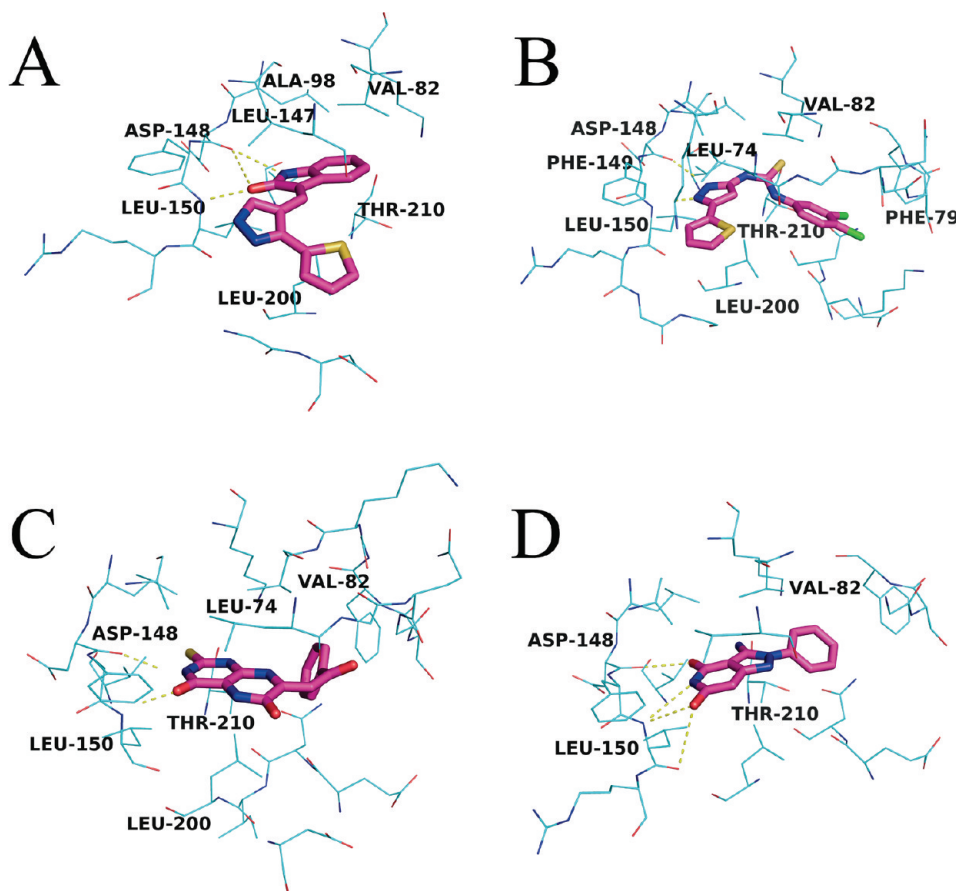


Figure 8. Binding models of representative hits. Binding of compounds (stick mode, purple carbon) **10** (A), **12** (B), **14** (C), and **16** (D) in the final RSK2 NTKD model (wire, cyan carbon) is illustrated. Nitrogen and oxygen atoms are colored blue and red, respectively. Hydrogen atoms are hidden for clarity. Potential intermolecular hydrogen bonds are shown as yellow dashed lines.

similar inhibitory activities (3.89 and 2.4 μM , respectively), because they are chemical analogues. Similar to compound **10**, compound **12**, which also has a pyrazole moiety, can form two hydrogen bonds with Asp148 and Leu150 (Figure 8B). The phenyl moiety of Phe79, the hydroxyl group of Thr210, the isopropyl moiety of Val82, and the dichlorobenzene moiety of compound **12** interact with each other, resulting in a strongly hydrophobic region. The thiophene moiety, which is directly connected to the ring of the pyrazole, tightly interacts with the isobutyl moieties of Leu74 and Leu200 as well as the phenyl group of Phe149, through VDW and hydrophobic interactions. Compound **14** (Figure 8C) can also form hydrogen bonds with Asp148 and Leu150 simultaneously. In addition, a favorable hydrophobic region is formed by Val82, Leu200, Thr210, and the phenyl moiety of compound **14**. An enol–keto tautomerism exists in compound **16** (Figure 8D), resulting in the more stable structure of glutarimide, which may reinforce the hydrogen bonds formed with Asp148 and Leu150 in the hinge region. The phenyl moiety can also form hydrophobic and VDW interactions with Val82 and Thr210.

After the detailed analysis of the binding modes for the seven newly discovered inhibitors, common binding motifs can be extracted. First, there is usually one or two hydrogen bonds formed between the ligands and the hinge residues (Asp148 and Leu150), with a rigid moiety occupying the adenine region of the ATP-binding site of the RSK2 NTKD. Second, two hydrophobic

regions exist in the ATP-binding site to provide hydrophobic interactions and VDW contacts with the inhibitors. One of these consists of Leu74, Ala98, Phe149, and Leu200, while the other comprises Phe79, Val82, Val131, Leu147, and Thr210. Observing these general features will be essential for further structure-based hit optimization.

CONCLUSIONS

In summary, a structurally reasonable and energetically reliable RSK2 NTKD model was built with homology modeling and a subsequent stepwise refinement procedure by docking the known inhibitors into the ATP-binding site of the initial model. Using the refined model, structure-based virtual screening was performed, and seven novel RSK2 inhibitors were identified with IC_{50} values ranging from 2.4 to 14.45 μM . In addition, the detailed binding modes of the seven novel molecules were analyzed, laying a solid foundation for further structure-based hit-to-lead optimization.

ASSOCIATED CONTENT

S Supporting Information. Ranking and scoring results by GlideScore for the 26 candidate compounds selected from virtual screening for activity test are listed in Table S1. Final RSK2 NTKD atomic model in complex with the five known ligands in

PDB format is also attached. This information is available free of charge via the Internet at <http://pubs.acs.org>.

AUTHOR INFORMATION

Corresponding Author

*E-mail: huangjin@ecust.edu.cn; xxfliu@gmail.com.

Author Contributions

[§] Authors contributed equally to this work.

ACKNOWLEDGMENT

This work was supported by the National Natural Science Foundation of China (grants 20803022, 21173076, and 81102375), the Shanghai Committee of Science and Technology (grants 09dZ1975700 and 10431902600), the Innovation Program of Shanghai Municipal Education Commission (grant 10ZZ41), the National S&T Major Project of China (grant 2011-ZX09307-002-03), and the Fundamental Research Funds for the Central Universities. H. Li is also sponsored by the Shanghai Rising-Star Program (grant 10QA1401800) and the Program for New Century Excellent Talents in University (grant NCET-10-0378). We also thank Prof. Rolf Hilgenfeld from University of Lübeck for careful reading and polishing of this manuscript.

REFERENCES

- (1) Clark, D. E.; Errington, T. M.; Smith, J. A.; Frierson, H. F.; Weber, M. J.; Lannigan, D. A. The serine/threonine protein kinase, p90 ribosomal S6 kinase, is an important regulator of prostate cancer cell proliferation. *Cancer Res.* **2005**, *65* (8), 3108–3116.
- (2) Lee, K. Y.; Bignone, P. A.; Ganesan, T. S. p90 ribosomal S6 kinases - eclectic members of the human kinome. *Signal Transduction* **2007**, *7* (3), 225–239.
- (3) Gioeli, D.; Mandell, J. W.; Petroni, G. R.; Frierson, H. F.; Weber, M. J. Activation of mitogen-activated protein kinase associated with prostate cancer progression. *Cancer Res.* **1999**, *59* (2), 279–284.
- (4) Pereira, P. M.; Schneider, A.; Pannetier, S.; Heron, D.; Hanauer, A. Coffin-Lowry syndrome. *Eur. J. Hum. Genet.* **2010**, *18* (6), 627–633.
- (5) Touraine, R. L.; Zeniou, M.; Hanauer, A. A syndromic form of X-linked mental retardation: the Coffin-Lowry syndrome. *Eur. J. Pediatr.* **2002**, *161* (4), 179–187.
- (6) Jurkiewicz, D.; Jezela-Stanek, A.; Ciara, E.; Pieikutowska-Abramczuk, D.; Kugando, M.; Gajdlewicz, M.; Chrzanowska, K.; Popowska, E.; Krajewska-Walasek, M. Four novel RSK2 mutations in females with Coffin-Lowry syndrome. *Eur. J. Med. Genet.* **2010**, *53* (5), 268–273.
- (7) Falco, M.; Romano, C.; Alberti, A.; Greco, D.; Scuderi, C.; Avola, E.; Failla, P.; Belli, S.; Tolmie, J. L.; Amata, S.; Fichera, M. Identification of novel mutations in patients with Coffin-Lowry syndrome by a denaturing HPLC-based assay. *Clin. Chem.* **2005**, *51* (12), 2356–2358.
- (8) Lu, W.; Liu, X.; Cao, X.; Xue, M.; Liu, K.; Zhao, Z.; Shen, X.; Jiang, H.; Xu, Y.; Huang, J.; Li, H. SHAFTS: a hybrid approach for 3D molecular similarity calculation. 2. Prospective case study in the discovery of diverse p90 ribosomal S6 protein kinase 2 inhibitors to suppress cell migration. *J. Med. Chem.* **2011**, *54* (10), 3564–3574.
- (9) Jones, S. W.; Erikson, E.; Blenis, J.; Maller, J. L.; Erikson, R. L. A *Xenopus* ribosomal protein S6 kinase has two apparent kinase domains that are each similar to distinct protein kinases. *Proc. Natl. Acad. Sci. U.S.A.* **1988**, *85* (10), 3377–3381.
- (10) Chrestensen, C. A.; Sturgill, T. W. Characterization of the p90 ribosomal S6 kinase 2 carboxyl-terminal domain as a protein kinase. *J. Biol. Chem.* **2002**, *277* (31), 27733–27741.
- (11) Xing, J.; Ginty, D. D.; Greenberg, M. E. Coupling of the RAS-MAPK pathway to gene activation by RSK2, a growth factor-regulated CREB kinase. *Science* **1996**, *273* (5277), 959–963.
- (12) Sassone-Corsi, P.; Mizzen, C. A.; Cheung, P.; Crosio, C.; Monaco, L.; Jacquot, S.; Hanauer, A.; Allis, C. D. Requirement of RSK-2 for epidermal growth factor-activated phosphorylation of histone H3. *Science* **1999**, *285* (5429), 886–891.
- (13) Cho, Y.-Y.; He, Z.; Zhang, Y.; Choi, H. S.; Zhu, F.; Choi, B. Y.; Kang, B. S.; Ma, W.-Y.; Bode, A. M.; Dong, Z. The p53 protein is a novel substrate of ribosomal S6 kinase 2 and a critical intermediary for ribosomal S6 kinase 2 and histone H3 interaction. *Cancer Res.* **2005**, *65* (9), 3596–3603.
- (14) Silverman, E.; Frodin, M.; Gammeltoft, S.; Maller, J. L. Activation of p90RSK1 is sufficient for differentiation of PC12 cells. *Mol. Cell. Biol.* **2004**, *24* (24), 10573–10583.
- (15) Schwab, M. S.; Roberts, B. T.; Gross, S. D.; Tunquist, B. J.; Taieb, F. E.; Lewellyn, A. L.; Maller, J. L. Bub1 is activated by the protein kinase p90^{RSK} during *Xenopus* oocyte maturation. *Curr. Biol.* **2001**, *11* (3), 141–150.
- (16) Chen, R. H.; Abate, C.; Blenis, J. Phosphorylation of the c-Fos transrepression domain by mitogen-activated protein kinase and 90-kDa ribosomal S6 kinase. *Proc. Natl. Acad. Sci. U.S.A.* **1993**, *90* (23), 10952–10956.
- (17) Swanson, K. D.; Taylor, L. K.; Haung, L.; Burlingame, A. L.; Landreth, G. E. Transcription factor phosphorylation by pp90 RSK2. *J. Biol. Chem.* **1999**, *274* (6), 3385–3395.
- (18) Doebe, U.; Hauge, C.; Frank, S. R.; Jensen, C. J.; Duda, K.; Nielsen, J. V.; Cohen, M. S.; Johansen, J. V.; Winther, B. R.; Lund, L. R.; Winther, O.; Taunton, J.; Hansen, S. H.; Frödin, M. RSK as a principal effector of the RAS-ERK pathway for eliciting a coordinate promotile/invasive gene program and phenotype in epithelial cells. *Mol. Cell* **2009**, *35* (4), 511–522.
- (19) Malakhova, M.; Tereshko, V.; Lee, S.-Y.; Yao, K.; Cho, Y.-Y.; Bode, A.; Dong, Z. Structural basis for activation of the autoinhibitory C-terminal kinase domain of p90 RSK2. *Nat. Struct. Mol. Biol.* **2008**, *15* (1), 112–113.
- (20) Nguyen, T. L.; Rick, G.; Smith, J. A. Homology model of RSK2 N-terminal kinase domain, structure-based identification of novel RSK2 inhibitors, and preliminary common pharmacophore. *Bioorg. Med. Chem.* **2006**, *14* (17), 6097–6105.
- (21) Nguyen, T. L. Targeting RSK: an overview of small molecule inhibitors. *Anti-Cancer Agents Med. Chem.* **2008**, *8* (7), 710–716.
- (22) Discovery Studio, version 2.1; Accelrys, Inc.: San Diego, CA, 2008; <http://accelrys.com/>. Accessed December 5, 2009.
- (23) Laskowski, R. A.; MacArthur, M. W.; Moss, D. S.; Thornton, J. M. PROCHECK: a program to check the stereochemical quality of protein structures. *J. Appl. Crystallogr.* **1993**, *26* (2), 283–291.
- (24) Laskowski, R. A.; Rullmann, J. A. C.; MacArthur, M. W.; Kaptein, R.; Thornton, J. M. AQUA and PROCHECK-NMR: Programs for checking the quality of protein structures solved by NMR. *J. Biomol. NMR* **1996**, *8* (4), 477–486.
- (25) Procheck; European Bioinformatics Institute: Cambridge, U.K.; http://nihserver.mbi.ucla.edu/SAVES_3/. Accessed March 12, 2009.
- (26) Laskowski, R. A.; MacArthur, M. W.; Thornton, J. M. Validation of protein models derived from experiment. *Curr. Opin. Strut. Biol.* **1998**, *8* (5), 631–639.
- (27) Prime, version 1.5; Schrödinger, LLC: New York, NY, 2005; <http://www.schrodinger.com/>. Accessed December 3, 2009.
- (28) Maestro, version 7.5; Schrödinger, LLC: New York, NY, 2005; <http://www.schrodinger.com/>. Accessed December 3, 2009.
- (29) Glide, version 4.0; Schrödinger, LLC: New York, NY, 2005; <http://www.schrodinger.com/>. Accessed December 3, 2009.
- (30) Maybridge; Fisher Scientific: Pittsburgh, PA; <http://www.maybridge.com/>. Accessed April 12, 2010.
- (31) LigPrep, version 2.0; Schrödinger, LLC: New York, NY, 2005; <http://www.schrodinger.com/>. Accessed December 3, 2009.
- (32) Pipeline Pilot, version 7.5; Accelrys: San Diego, CA, 2008; <http://accelrys.com/products/scitelic/>. Accessed April 17, 2010.

(33) Cho, Y.-Y.; Yao, K.; Pugliese, A.; Malakhova, M. L.; Bode, A. M.; Dong, Z. A Regulatory Mechanism for RSK2 NH₂-Terminal Kinase Activity. *Cancer Res.* **2009**, *69* (10), 4398–4406.

(34) *Geneious*, Version 4.7.4; Biomatters, Ltd.: Auckland, New Zealand, 2009; <http://www.geneious.com/>. Accessed December 3, 2009.